KLOE-2 Collaboration - LNF Group

D. Babusci, C. Bloise, F. Bossi, G. Capon (Ass.), E. De Lucia (Resp.), A. De Santis, P. De Simone, G. Fortugno (Tec.), S. Giovannella, M. Martini (Ass)*, S. Miscetti, P. Santangelo, F. Sborzacchi (Tec.).

Also Dipartimento di Scienze e Tecnologie applicate,"Guglielmo Marconi" University, Rome, Italy

1 Introduction

KLOE and KLOE-2 data set, about 2.4×10^{10} ϕ-meson produced, provides the largest sample ever collected at the $\phi(1020)$ meson peak at e^+e^- colliders. The physics program is focused on fundamental symmetry tests and physics beyond the Standard Model, including kaon interferometry and searches for new exotic particles that could constitute the dark matter, together with K_S and η meson rare decays. Activities are mainly concentrated on data reconstruction and analysis towards precise measurements in both kaon and hadron sectors. Data reconstruction have been completed for the whole data set together with the production of a luminosity equivalent MC sample. The production of the ROOT output for KLOE-2 data, according to the experiment long-term Data Preservation plan, was completed exploiting the features of the experiment CED expanded and renewed for Data Consolidation. Within the Data Preservation plan, the KLOE-2 CED completed Data Migration from the old IBM3494 to the new TS4500 tape library together with copy of the almost 70% of the RAW data into the disaster recovery LTO tape library.

KLOE-2 Collaboration published in 2022 the paper on Precision tests of Quantum Mechanics and CPT symmetry with entangled neutral kaons [1]. From the fit of the observed Δt distribution, being Δt the difference of the kaon decay times, the decoherence and CPT violation parameters of various phenomenological models are measured with a largely improved accuracy with respect to previous analyses, providing the most stringent limits up to date on the considered models.

Latest physics results achieved in 2022 are: i) a new measurement of the KSe3 branching fraction, ii) the final results on the direct test of T and CPT symmetries in neutral kaon transitions, iii) the final result on the $\eta \to \pi^0\gamma\gamma$ decay branching ratio, one of the golden tests of Chiral Perturbation Theory, which agrees with the previous KLOE preliminary result at $1.2\,\sigma$ level, confirming the discrepancy with the Crystal Ball measurement, iv) statistical evidence of correlated coincidence events with a precision of about 7% has been observed in the search for candidates of single-π^0 production from $\gamma\gamma$ scattering with 3 fb^{-1} KLOE-2 data, v) the final invariant mass distributions from $\phi \to \eta B \to \eta\pi^0\gamma$ to search for the B-boson, a leptophobic mediator between the dark sector and the Standard Model.

These measurements together with preliminary results from other ongoing analysis, both with KLOE and KLOE-2 samples, have been presented at several international conferences and workshops including ICHEP2022, QNP2022, Excited QCD, PhiPsi2022, eeFACT2022, KAON2022 and DISCRETE2022.

2 Data Reconstruction and MC simulation

During 2022 the final round of data processing was completed with a total 5.1 fb^{-1} reconstructed with the improved version of the official reconstruction software, so-called DBV-40. The simulation and reconstruction of the full data set was also completed in 2022, providing a luminosity scale factor LSF=1 sample with main ϕ-meson decays. According to the KLOE-2 long-term Data Preservation plan, along with the reconstruction of the data and the simulation, a ROOT output

of the reconstructed data is being produced. The ROOT file creation relays on the already reconstructed data with the DBV-40 and is inexpensive in terms of CPU time. ROOT output for KLOE-2 data was completed in 2022 with neutral kaons, charged kaons, radiative decays and $\rho\pi$ streams produced with a compression factor of about 8, depending on run conditions. Present effort is in the production of the ROOT output for KLOE-2 MC and KLOE data. To facilitate analysis, the ROOT files will be kept on disk and to this purpose 400 TB were funded by INFN-CSN1 committee and have been purchased.

3 CED

During the last year, beside the usual activities, KLOE-2 CED carried on some significant consolidation and preservation tasks, started in 2019 and continued during 2020-2021, together with others related to the system management. *Data Preservation* went ahead intermittently, due to the heavy data analysis and data reconstruction activity, moving the precious KLOE and KLOE-2 raw data from both the old IBM3494 and new TS4500 tape libraries to a disaster recovery LTO tape library.

The whole data-set has been copied, while the reconstruction and analysis were going on, from the old IBM3494 tape library and 70% of the raw data has been copied into LTO tape. The data preservation task will require several months in 2023 to be accomplished. We are validating the data transferred from old library into the database entries as last check before switching off the old library IBM3494, this will require about three months to be accomplished.

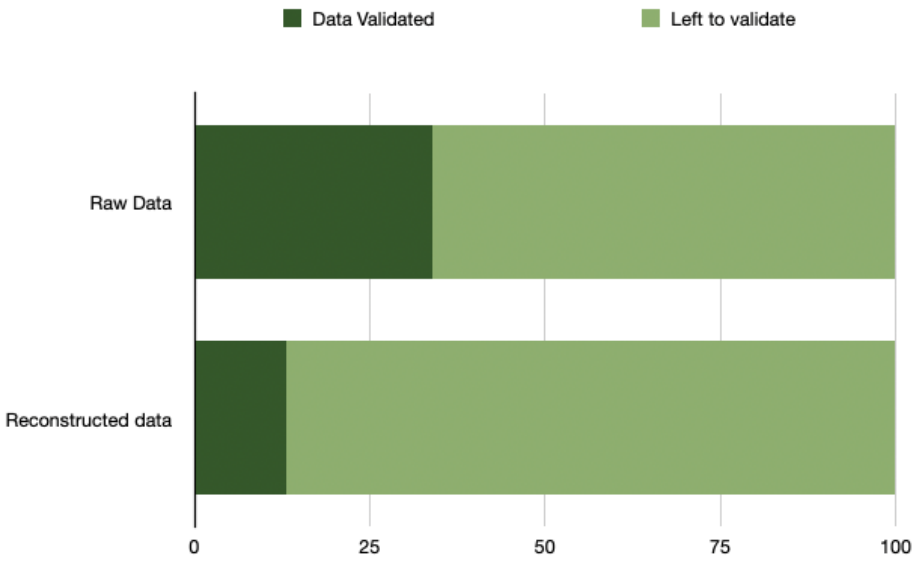

Figure 1: KLOE CED Data consolidation and Data preservation rate

The disk infrastructure has become faster, with the introduction of new high capacity SSD disk on top of the tiering level. Always managed with the GPFS protocol, with two different disk arrays controlled by IA. Both arrays achieve the wonderful rank of 8 Gigabyte per second of total throughput. The throughput is very high also when our cluster is working at full rank, with 800 different reconstruction and analysis jobs which make IO activities up to 80000 files at the same time. The AI is able to keep under 2 ms the latency of the access to storage data. This result allow

us to have no wait time related to programs concerning the IO of the operative system on every node of the cluster. Therefore we are free to saturate the CPU available without the slowdown of the Input Output system. This result has been reached and fixed with software and hardware both focused to keep the speed in every working condition. The redundant Storage Area Network with fibre channel protocol and the GPFS protocol managing the disk array controlled by IA, caching system with hierarchical device tiering, make the infrastructure so strong to work for many weeks without interruption and without slowing down the efficiency or decreasing the throughput level.

The job submission system, based upon GPFS file system, managed more than 140.000 jobs during the last year without missing even a single job. It dispatched and managed more efficiently the load into the KLOE-2 computing cluster, working as a High Performance Computing in parallel way with a high level of latency. This cluster with the new job submission system is the keystone of the KLOE-2 tasks, fitting the jobs to the cluster resources without making over heading even a single processor, so to keep the efficiency at the top level. The analysis, the reconstruction and the Monte Carlo production are now managed by the submission system with different priority, altered every time the KLOE-2 collaboration changed the priority of the different tasks involved.

The structure of KLOE-2 CED has become more compact and efficient, reliable and reactive to the user's requests with the GPFS as a new data distribution centre. Every client has a multi-path channel to read and write data guaranteed as speed, to reduce the wait time for every IO operation. The increase in terms of speed is the cornerstone of the new architecture, started in 2019 and completed during 2020. This consolidated architecture with the storage area network, allows for every task, to reach the best level of efficiency and beside has deployed a new data redundant distribution system. This redundant architecture led to zero the number of jobs slowed down due to disks I/O congestion. The AI and the SDD disk tearing level, deploy at the highest access performance for writing programs.

Night and day, there is an AI working to organise and optimise the access to files belonging to the array. The AI is moving files in and out from the three caching levels with the purpose to minimise the access time and, as shown in the Fig.2 and Fig.3, the results are very good before the SSD upgrade and outstanding after the upgrade. Every time the AI model controlling the file

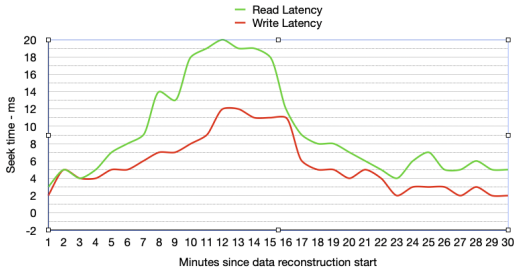

Figure 2: Disk Arrays read/write latency before update.

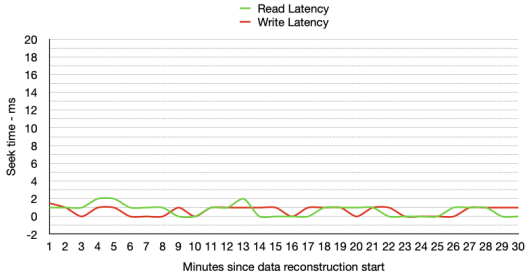

Figure 3: Disk Arrays read/write latency now.

distribution is becoming more expert of our file usage and the files necessary to jobs running into the HPC cluster are managing to increase the speed and lower the access time. Now, every job running on the cluster works without interference from other jobs, like as if it was alone in the cluster. The algorithm of the AI designed to satisfy the file hungry jobs have suited to our typical job request and is becoming every day better in its tasks.

The Storage Area Network is the other improvement of the CED. We changed two old CISCO switches with new ones and moved from 16 Gbit to 32 Gbit new interfaces, increasing the total

throughput by a factor of 4. The new CISCO fibre channel switches allow both tape and disk array interfaces to work at full speed. Because the port interfaces of the tape drive or the disk arrays cannot be increased by number, reaching the full speed is a good enhancement for our storage network. We can also increase, in this way, the maximum number of files exchanged from programs to devices or from device to device. Now in a normal run with HPC cluster, the storage area network can manage more than 150.000 file simultaneously without delays due to IO wait times. Our Storage Network can face challenging tasks like physics modelling or parallel fluid-dynamics programs which represent the highest difficult programs level into the whole programming world. The environment required to run those programs, CPU and infrastructure, is now available into our cluster. So, we managed the tasks required from KLOE-2 experiment reconstruction and analysis in a powerful environment act to solve every request needed. Continuous studies for a new computational model have been developed with the not used power or during the idle time of the main tasks, because every simulation runs in a parallel environment extruded from the main one, partitioning resources and using them to bump not into one another.

4 Physics achievements

In the following sections latest achievements obtained analysing the unique data sample collected by KLOE and KLOE-2 experiments will be discussed, in both kaon and hadron sectors.

4.1 $K_S \to \pi e \nu$ branching ratio measurement

The KLOE-2 Collaboration continues the KLOE long-standing tradition of flavour physics precision measurements in the kaon sector with a new $K_S \to \pi e \nu$ branching fraction measurement with 1.63 fb^{-1} KLOE data acquired at DAΦNE. Branching fraction measurements for semileptonic decays of charged and neutral kaons together with their lifetimes are used to determine the $|V_{us}|$ Cabibbo–Kobayashi–Maskawa quark mixing matrix element [3, 4, 5]. Lately an apparent 3.2σ violation of the first-row CKM unitarity condition $|V_{ud}|^2+|V_{us}|^2+|V_{ub}|^2 = 1$ has been reported, using the most recent inputs from theory and experiment to extract the V_{us} value from $K_{\ell 3}$ decays and the V_{ud} value from superallowed nuclear beta decays [2]. Given the lack of pure high-intensity K_S meson beams, $K_S \to \pi l \nu$ decays provide the least precise determination of $|V_{us}|$ compared to $K^{\pm}$ and K_L mesons [4], with the first direct measurement ever of the branching fraction $\mathcal{B}(K_S \to \pi \mu \nu)$ published by the our collaboration [6]. K_S (K_L) mesons produced at DAΦNE in $\phi \to K_L K_S$ decays are (*tagged*) by the presence of a K_L (K_S) in the opposite hemisphere. Exploiting this unique capability of selecting pure K_S beams, we have analyzed about 300 million K_S mesons to improve the precision on the $K_S \to \pi e \nu$ branching fraction measurement [7]. The $K_S \to \pi e \nu$ signal selection exploits a boosted decision tree (BDT) classifier built with kinematic variables measured with DC only (Fig.4) together with time-of-flight measurements from EMC. The signal yield is provided by the fit to the reconstructed electron mass distribution (Fig.5) which is then normalised to $K_S \to \pi^+\pi^-$ decays in the same data set. $K_L \to \pi e \nu$ data control samples are used to evaluate signal selection efficiencies. The master formula for the evaluation of the $K_S \to \pi e \nu$ branching fraction is:

$$\mathcal{B}(K_S \to \pi e \nu) = \frac{N_{\pi e \nu}}{\epsilon_{\pi e \nu}} \times \frac{\epsilon_{\pi\pi}}{N_{\pi\pi}} \times R_\epsilon \times \mathcal{B}(K_S \to \pi^+\pi^-), \quad (1)$$

with $N_{\pi e \nu}$ and $N_{\pi\pi}$ the selected $K_S \to \pi e \nu$ and $K_S \to \pi^+\pi^-$ events, $\epsilon_{\pi e \nu}$ and $\epsilon_{\pi\pi}$ the selection efficiencies, and $R_\epsilon = (\epsilon_{\pi\pi}/\epsilon_{\pi e \nu})_{\rm com}$ the ratio of common efficiencies that can be different for the two decays.
With $N_{\pi e \nu} = 49647 \pm 316$ events, $\epsilon_{\pi e \nu} = (19.38 \pm 0.10)$, $N_{\pi\pi}/\epsilon_{\pi\pi} = (292.08 \pm 0.27) \times 10^6$, $R_\epsilon =$

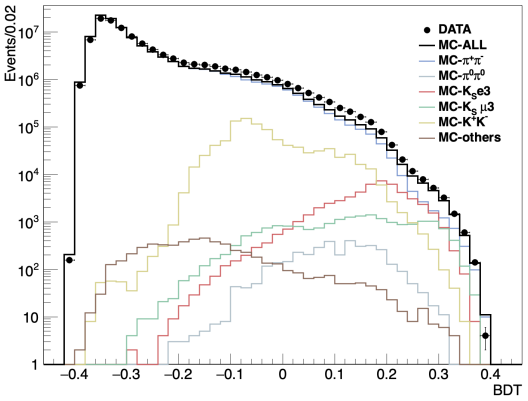

Figure 4: The BDT classifier output for data and MC signal and background components.

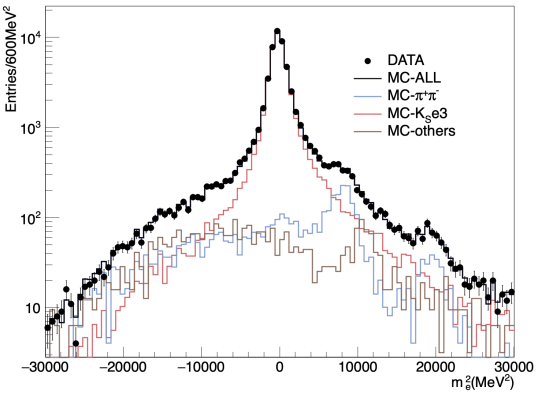

Figure 5: The m_e^2 distribution for data, MC signal and background compared with the fit result.

1.1882 ± 0.0059 and $\mathcal{B}(K_S \to \pi^+\pi^-) = 0.69196 \pm 0.00051$ measured by KLOE [8], the branching fraction has been evaluated: $\mathcal{B}(K_S \to \pi e\nu) = (7.211 \pm 0.046_{\rm stat} \pm 0.052_{\rm syst}) \times 10^{-4}$ with an overall uncertainty below 1%. Combining this new result with our previous BR($K_S \to \pi e\nu$) measurement, based on a 0.41 fb^{-1} independent data sample [9], allows a 0.8% precision to be reached improving by almost a factor of two:

$$\mathcal{B}(K_S \to \pi e\nu) = (7.153 \pm 0.037_{\rm stat} \pm 0.043_{\rm syst}) \times 10^{-4} = (7.153 \pm 0.057) \times 10^{-4}.$$

The corresponding new derivation of the $f_+(0)|V_{us}|$ value is done with the equation:

$$\mathcal{B}(K_S \to \pi\ell\nu) = \frac{G^2 (f_+(0)|V_{us}|)^2}{192\pi^3} \tau_S m_K^5 I_K^\ell S_{\rm EW} (1 + \delta_{\rm EM}^{K\ell}),$$

with I_K^ℓ the phase-space integral including the semileptonic form factors, $S_{\rm EW}$ the short-distance electro-weak correction, $\delta_{\rm EM}^{K\ell}$ the mode-dependent long-distance radiative correction, and $f_+(0)$ the form factor at zero momentum transfer for the $\ell\nu$ system. With the values $S_{\rm EW} = 1.0232 \pm 0.0003$ [10], $I_K^e = 0.15470 \pm 0.00015$ and $\delta_{\rm EM}^{Ke} = (1.16 \pm 0.03)\ 10^{-2}$ from Ref. [2], and the world average values for the K_S mass and lifetime [5] we have:

$$f_+(0)|V_{us}| = 0.2170 \pm 0.0009.$$

with a sizable reduction with respect to previous value, from 0.6% to 0.4%.

4.2 Direct test of T and CPT symmetries in neutral kaon transitions

Tests of the T, CP and CPT symmetries in the neutral kaon system have been performed by the direct comparison of the probabilities of a kaon transition process to its symmetry-conjugate. The comparison of neutral meson transition rates between flavour and CP eigenstates allows direct and model independent tests of time-reversal T and CPT symmetries [11] to be performed. To identify the initial state of a particle transition by the decay of its entangled partner, quantum entangled kaon pairs are used. The final state instead is tagged by semileptonic and hadronic decays into two and three pions.
About 1.7 fb^{-1} integrated luminosity has been analysed to study the Δt distributions of the

$K_S K_L \to \pi^{\pm} e^{\mp} \nu, 3\pi^0$ and $K_S K_L \to \pi^+\pi^-, \pi^{\pm} e^{\mp} \nu$ processes, with Δt the difference of the kaon decay times. A comparison of the measured Δt distributions in the asymptotic region $\Delta \mathrm{t} >> \tau_{\mathrm{S}}$ allows to test for the first time T and CPT symmetries in kaon transitions with a precision of few percent, and to observe CP violation with this novel method.
T-violation can be tested through the following ratios of the rates of two classes of processes identified in the dataset:

$$\mathrm{R}_2(\Delta t) = \frac{\mathrm{P}[\mathrm{K}^0(0) \to \mathrm{K}_-(\Delta t)]}{\mathrm{P}[\mathrm{K}_-(0) \to \mathrm{K}^0(\Delta t)]} \sim \frac{\mathrm{I}(\pi^+ e^- \bar{\nu}, 3\pi^0; \Delta t)}{\mathrm{I}(\pi^+\pi^-, \pi^- e^+ \nu; \Delta t)}, \tag{2}$$

$$\mathrm{R}_4(\Delta t) = \frac{\mathrm{P}[\bar{\mathrm{K}^0}(0) \to \mathrm{K}_-(\Delta t)]}{\mathrm{P}[\mathrm{K}_-(0) \to \bar{\mathrm{K}^0}(\Delta t)]} \sim \frac{\mathrm{I}(\pi^- e^+ \nu, 3\pi^0; \Delta t)}{\mathrm{I}(\pi^+\pi^-, \pi^+ e^- \bar{\nu}; \Delta t)}, \tag{3}$$

with I(f_1,f_2;Δt) denoting the number of recorded events characterized by a time-ordered pair of kaon decays f_1 and f_2 separated by an interval of proper kaon decay times Δt [11]. A deviation from unity of the asymptotic level of these ratios at large transition time values would be a T-violation manifestation.

To test CPT symmetry, the determination of the asymptotic level of the following double ratio is used:

$$\frac{R_2^{CPT}}{R_4^{CPT}} = \frac{\mathrm{P}[\mathrm{K}^0(0) \to \mathrm{K}_-(\Delta t)]/\mathrm{P}[\mathrm{K}_-(0) \to \bar{\mathrm{K}^0}(\Delta t)]}{\mathrm{P}[\bar{\mathrm{K}^0} \to \mathrm{K}_-(\Delta t)]/\mathrm{P}[\mathrm{K}_-(0) \to \mathrm{K}^0(\Delta t)]} \overset{\Delta t \gg \tau_S}{=} 1 - 8Re(\delta) - 8Re(x_-), \tag{4}$$

with δ and x_- being the parameters violating CPT symmetry in $\mathrm{K}^0\bar{\mathrm{K}^0}$ mixing and the $\Delta S = \Delta Q$ rule, respectively. This double ratio represents a robust CPT-violation sensitive observable [11] which has never been measured to date.

Event selection efficiencies have been evaluated using Monte Carlo simulations and data/MC corrections based on reference channels where necessary. Rates of the aforementioned two classes of processes, expressed as a function of the difference of proper kaon decay times, were compared to obtain T, CP and CPT -violation sensitive observables. The time-dependent rates were fit in the asymptotic time difference range ($\Delta t >> \tau_{\mathrm{S}}$) with a maximum likelihood fit, yielding the following results [12]:

$$\begin{aligned}
R_2^T &= 0.991 \pm 0.017_{\mathrm{stat}} \pm 0.014_{\mathrm{syst}} \pm 0.012_{\mathrm{D}}, \\
R_4^T &= 1.015 \pm 0.018_{\mathrm{stat}} \pm 0.015_{\mathrm{syst}} \pm 0.012_{\mathrm{D}}, \\
R_2^{CPT} &= 1.004 \pm 0.017_{\mathrm{stat}} \pm 0.014_{\mathrm{syst}} \pm 0.012_{\mathrm{D}}, \\
R_4^{CPT} &= 1.002 \pm 0.017_{\mathrm{stat}} \pm 0.015_{\mathrm{syst}} \pm 0.012_{\mathrm{D}}, \\
R_2^{CP} &= 0.992 \pm 0.028_{\mathrm{stat}} \pm 0.019_{\mathrm{syst}}, \\
R_4^{CP} &= 1.00665 \pm 0.00093_{\mathrm{stat}} \pm 0.00089_{\mathrm{syst}}, \\
R_2^T/R_4^T &= 0.979 \pm 0.028_{\mathrm{stat}} \pm 0.019_{\mathrm{syst}}, \\
R_2^{CPT}/R_4^{CPT} &= 1.005 \pm 0.029_{\mathrm{stat}} \pm 0.019_{\mathrm{syst}}.
\end{aligned}$$

where D denotes the uncertainty on the factor $\mathrm{D} = \mathrm{BR}(K_L \to 3\pi^0)\tau_S/\mathrm{BR}(K_S \to \pi^+\pi^-)\tau_L$.
Fig. 6 and Fig. 7 show T- and CPT-violation sensitive ratios of double decay rates respectively. Double ratios of double kaon decay rates sensitive to effects of T violation and CPT violation are reported in Fig. 8. Fig. 9 shows the comparison of the measured symmetry-violation-sensitive single and double ratios and their expected values (horizontal dashed lines) assuming CPT invariance and T violation extrapolated from observed CP violation in the mixing. Solid error bars denote

statistical uncertainties and dotted error bars represent total uncertainties (including error on the D factor in case of single T and CPT-violation sensitive ratios). The right-hand-side panel magnifies the region of the CP-violation-sensitive ratio R4,CP.

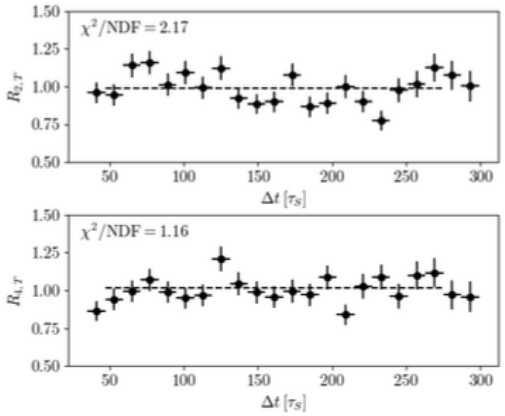

Figure 6: T-violation sensitive ratios of double decay rates as defined in Eq.2 and Eq. 3. Dashed lines denote levels obtained with the fit.

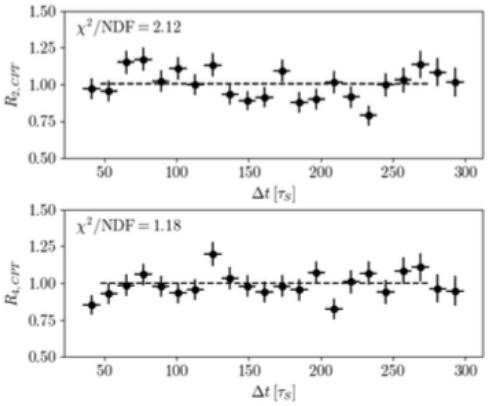

Figure 7: CPT-violation sensitive ratios of double decay rates as defined in Eq. 4. Dashed lines denote levels obtained with the fit.

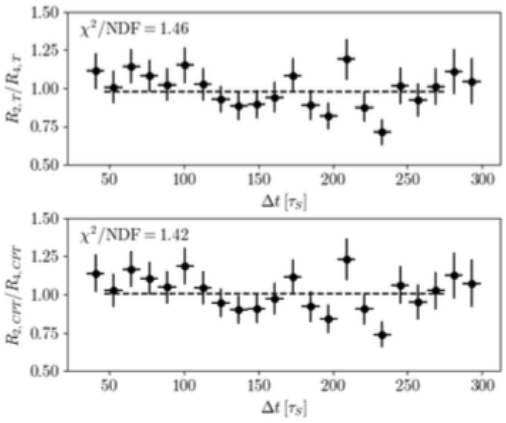

Figure 8: Double ratios of double kaon decay rates sensitive to effects of T violation (top) and CPT violation (bottom). Dashed lines denote levels obtained with the fit.

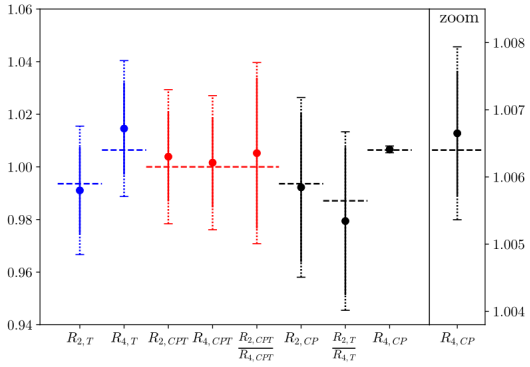

Figure 9: Measured symmetry-violation-sensitive single and double ratios and compared to their expected values (horizontal dashed lines) assuming CPT invariance and T violation extrapolated from observed CP violation in the mixing.

4.3 π^0 production from $\gamma\gamma$ scattering

The precision measurement of the $\pi^0 \to \gamma\gamma$ width would give insight into low-energy QCD dynamics. To achieve the $\mathcal{O}(1\%)$ precision needed to test theory predictions, KLOE-2 exploits the π^0

production through $\gamma\gamma$ fusion in the $e^+e^- \to e^+e^-\gamma^*\gamma^* \to e^+e^-\pi^0$ reaction [13]. To reduce the background from ϕ-meson decays, two High Energy Tagger (HET) stations [14] have been used to detect off-energy leptons scattered in the final state. The HET detectors, made up of 28 plastic scintillators, are installed in roman pots just at the exit of the DAΦNE dipole magnets, 11 m away from the interaction point (IP), both on positron and electron sides. HET scintillators are placed at different distances from the beam line, scintillators from 1 to 14 are on the horizontal plane of the machine while scintillators from 15 to 28 are displaced by a maximum of 2.8 mm in steps of 200 μm, to account for combined effects of the KLOE magnetic field and DAΦNE compensators on the off-energy particles.

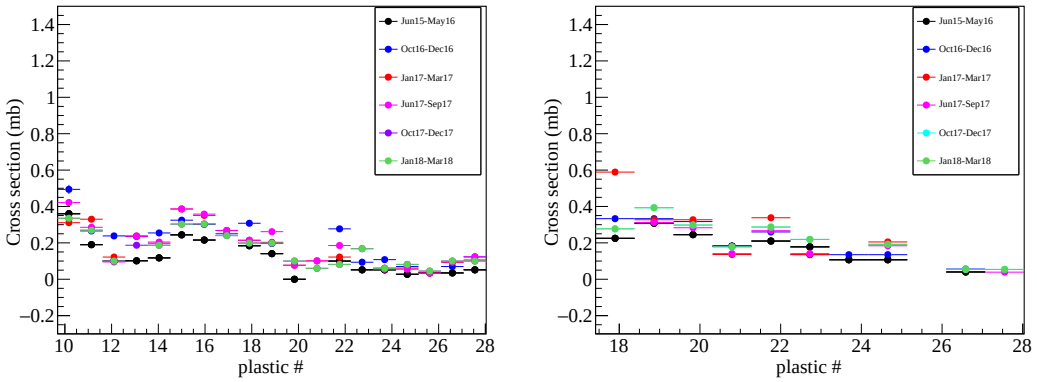

Figure 10: Effective low-angle radiative Bhabha cross-section per plastic as measured by the electron (left panel) and positron (right panel) stations in the whole data taking period.

The HET acquisition system has been designed to register more than two turns of the machine. Therefore, the time window of the HET data acquisition is wider than the KLOE-2 one ($\sim$ 250 ns) and varies from 660 to 970 ns. The $\gamma\gamma \to \pi^0$ signal is expected in the coincidence window between HET and KLOE-2 while the remaining buffer depth, acquired together with the coincidence sample, is used to evaluate the amount of uncorrelated time coincidences between the two detectors (accidentals).

The accidental counting rate is dominated by low-angle radiative Bhabha scattering and we use the effective cross-section, as a function of the data-taking period, to measure the detector acceptance×efficiency and for data quality.

Figure 10 shows the updated effective low-angle radiative Bhabha cross-section per plastic as measured by both stations in the whole HET electron and positron data sets, for the most stable plastic ranges 10–28 and 18–28 respectively. An effective total average cross-section of 2.5 $\pm$0.03 mb for the electron station and of 1.75 $\pm$0.024 mb has been measured for these plastics with data acquired between 2015 and 2018. The precision of the measurements has been improved increasing sample statistics by merging data-taking period showing a stable cross-section within the errors. A precision of few percent per HET plastic has been achieved. The intra-bunch scattering background as function of the data-taking period and per each plastic scintillator has been measured as well, the fraction varies from about 10 to 40% of the total measured HET rate according to the data-taking period.

For the π^0 search a sub-set of HET plastic scintillators has been used, chosen for their operational stability over a time scale of years. Candidates of single-π^0 production from $\gamma\gamma$ scattering have been pre-filtered recording information on the hit in the tagger, on the trigger signal, the

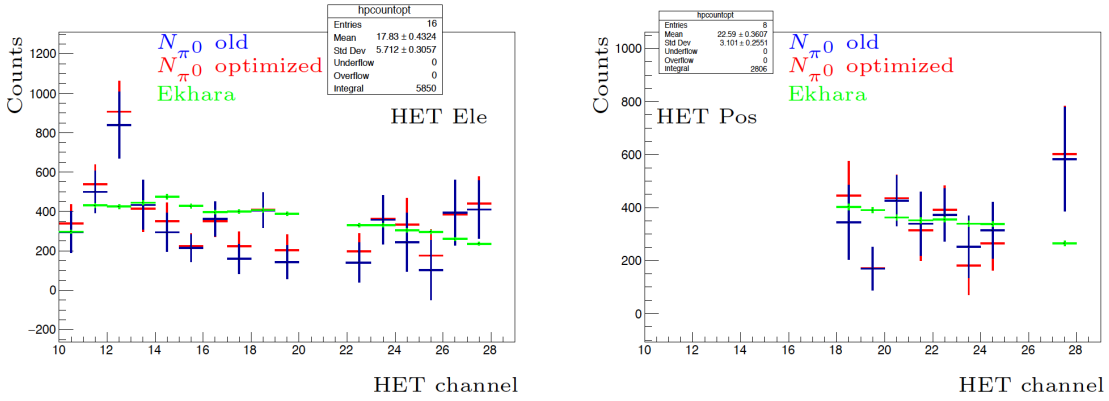

Figure 11: N_{π^0} counting per HET channel for both HET stations. The left plot refers to the HET electron station while the right plot shows result for the positron one. Blue points are π^0 tagged "weighted" to take into account differences in the measured efficiency along the data-taking. Red point are π^0 weighted events after counting fit procedure optimization. The green points represents Ekhara expectation for each channel.

DAΦNE operational parameters, clusters and tracks reconstructed in the KLOE-2 central detector. Data are classified as single-arm (SA) or double-arm (DA) events. DA events are selected requiring the time coincidence of the two HET stations within 12 ns, while for SA events, we selected hits in one HET station and at least one bunch in the KLOE-2 central detector associated with only 2 clusters in the calorimeter. Very loose kinematic cuts are applied to this sample. Statistical evidence of correlated coincidence events between the tagger station and the KLOE-2 calorimeter has been observed on whole reconstructed HET data sample of 3 fb^{-1}, on both electron and positron sides, with a precision of about 7% (merging both electron and positron samples) in a KLOE-HET coincidence window of a few bunches.

Fig. 11 shows the summary of the results obtained performing simultaneous fits on the KLOE-HET coincidence sample (A+ sample) in the $\Delta T_{\gamma\gamma} - \Delta R_{\gamma\gamma}/c$ vs $M_{\gamma\gamma}$ variables, per each HET channel. The A+ sample is constituted by a large amount of accidentals (A sample) and $\gamma\gamma \to \pi^0$ signal. Accidental events coming from ϕ-meson decays and surviving our selections have been totally rejected, using information derived from a study performed with GEANFI data. The accidental background is modeled using the HET data acquired out of the coincidence window with the KLOE-2 detector, while the $\gamma\gamma \to \pi^0$ signal is taken from the Ekhara simulation [15] interfaced with the BDSIM transport of leptons through the beam line [16]. A careful study of the calorimeter performance and of the trigger threshold has been performed, to properly model the expected $\gamma\gamma \to \pi^0$ signal. The π^0 counting fit procedure accounts also for differences in plastic response and global analysis efficiency $\epsilon_{\rm ana}$ which has been carefully evaluated along the data-taking (counting weighting). The fit procedure has been also recently optimized to improve as much as possible the quality of the fits obtaining consistent results. Significance tests on both measured and weighted counting results are in progress.

Moreover, studies have been performed to evaluate the sensitivity on the form factor slope measurement with the current HET data set. A toy MC based on Ekhara has been implemented and validated with simulated data. The study shows that the sensitivity achievable with the current analyzed data set in the region of interest ($Q^2 < 0.1$ GeV^2) is limited by signal statistics and kinematical cuts. A preliminary extraction of the Q^2 transferred to the not-tagged lepton per-

formed with both electron and positron data confirmed the conclusions from MC studies. For this reason, data have been processed again removing the tight kinematical cut on the total momentum P_{π^0} and releasing the cut on thecos $\theta_{\gamma\gamma}$ variable. The analysis of this new sample shows that the increasing of accidental background spoils the π^0 counting.

References

1. D. Babusci *et al.* [KLOE-2 Collaboration], JHEP04 (2022) 059 and https://doi.org/10.48550/arXiv.2111.04328
2. Seng C *et al* 2022 *Phys. Rev.* D **105** 013005
3. Antonelli A *et al* 2010 *Eur. Phys. J.* C **69** 399
4. Moulson M and Passemar E 2018 *DOI:10.5281/zenodo.2565479*
5. Zyla PA *et al* (Particle Data Group) 2020 *Prog. Theor. Exp. Phys.* 083C01
6. Babusci D *et al* 2020 *Phys. Lett.* B **804** 135378
7. Babusci D *et al* https://arxiv.org/abs/2208.04872v4
8. Ambrosino F *et al* 2006 *Eur. Phys. J.* C **48** 767
9. Ambrosino F *et al* 2006 *Phys. Lett.* B **636** 173
10. Marciano WJ and Sirlin A 1993 *Phys. Rev. Lett.* **71** 3629
11. Bernabeu, J., Di Domenico, A., Villanueva-Perez, P.: Direct test of time-reversal symmetry in the entangled neutral kaon system at a ϕ-factory. Nucl. Phys. B868, 102–119 (2013). https://doi.org/10.1016/j.nuclphysb.2012.11.009 and Bernabeu, J., Di Domenico, A., Villanueva-Perez, P.: Probing CPT in transitions with entangled neutral kaons. JHEP 10, 139 (2015). https://doi.org/10.1007/JHEP10(2015)139
12. Babusci D *et al* https://arxiv.org/abs/2211.12377v3
13. D. Babusci et al., Eur. Phys. J. C 72, 1917 (2012)
14. D. Babusci et al., Acta Phys. Pol B 46, 81 (2015)
15. H. Czyz, S. Ivashyn, Comput. Phys. Commun. 182 (2011)
16. I. Agapov, G.A. Blair, S. Malton, L. Deacon, Nucl. Instrum. Meth. A 606, 708 (2009)